J Biochem 128, 29–38 (2000)

Three-Dimensional Structure of 4-Amino-4-Deoxychorismate Lyase from *Escherichia coli*[1]

Tadashi Nakai,[*,2] Hisashi Mizutani,[*,2] Ikuko Miyahara,[*] Ken Hirotsu,[*,3] Sou Takeda,[†,2] Kwang-Hwan Jhee,[†,4] Tohru Yoshimura,[†] and Nobuyoshi Esaki[†]

[*]Department of Chemistry, Graduate School of Science, Osaka City University, Sumiyoshi-ku, Osaka 558-8585, and [†]Institute for Chemical Research, Kyoto University, Uji, Kyoto 611-0011

Received March 1, 2000; accepted April 10, 2000

4-Amino-4-deoxychorismate lyase (ADCL) is a member of the fold-type IV of PLP dependent enzymes that converts 4-amino-4-deoxychorismate (ADC) to *p*-aminobenzoate and pyruvate. The crystal structure of ADCL from *Escherichia coli* has been solved using MIR phases in combination with density modification. The structure has been refined to an *R*-factor of 20.6% at 2.2 Å resolution. The enzyme is a homo dimer with a crystallographic twofold axis, and the polypeptide chain is folded into small and large domains with an interdomain loop. The coenzyme, pyridoxal 5′-phosphate, resides at the domain interface, its *re*-face facing toward the protein. Although the main chain folding of the active site is homologous to those of D-amino acid and L-branched-chain amino acid aminotransferases, no residues in the active site are conserved among them except for Arg59, Lys159, and Glu193, which directly interact with the coenzyme and play critical roles in the catalytic functions. ADC was modeled into the active site of the unliganded enzyme on the basis of the X-ray structures of the unliganded and liganded forms in the D-amino acid and L-branched-chain amino acid aminotransferases. According to this model, the carboxylates of ADC are recognized by Asn256, Arg107, and Lys97, and the cyclohexadiene moiety makes van der Waals contact with the side chain of Leu258. ADC forms a Schiff base with PLP to release the catalytic residue Lys159, which forms a hydrogen bond with Thr38. The neutral amino group of Lys159 eliminates the α-proton of ADC to give a quinonoid intermediate to release a pyruvate in accord with the proton transfer from Thr38 to the olefin moiety of ADC.

Key words: aminodeoxychorismate lyase, pyridoxal enzyme, reaction mechanism, tertiary structure, X-ray structure.

In bacteria, chorismate serves as the branch point precursor for metabolites essential for the biosynthesis of many important aromatic products, such as anthranilate (precursor of tryptophan), prephenate (precursor of tyrosine or phenylalanine), *p*-aminobenzoate (precursor of folic acid), and *p*-hydroxybenzoate (precursor of ubiquinone) (*1*). Chorismate is converted into 4-amino-4-deoxychorismate (ADC) by *p*-aminobenzoate synthase encoded by *pabA* and *pabB*. Aminodeoxychorismate lyase (ADCL), which is a product of *pabC* and contains a tightly bound pyridoxal 5′-phosphate (PLP) as a cofactor, then converts ADC to *p*-aminobenzoate and pyruvate (Scheme 1) (*1–5*). Thus, ADCL is a key enzyme along with *p*-aminobenzoate synthase in the biosynthesis of *p*-aminobenzoate.

Based on the similarities in sequence, secondary structure, and hydropathy profiles, many PLP-dependent enzymes are placed in fold type I, while ADCL is placed in fold type IV together with D-amino acid aminotransferase (DAAT) and branched-chain amino acid aminotransferase (BCAT) (*6*). The sequence identities of *Escherichia coli* ADCL (eADCL) with *Bacillus* species YM-1 DAAT (bsDAAT) and *E. coli* BCAT (eBCAT) are 23 and 22%, respectively (*7*).

In most PLP-dependent enzymes, the catalytic residue lysine shuttles protons on the *si*-face of the planar π-system of the substrate-cofactor complex. However, enzymes belonging to fold type IV transfer protons on the *re*-face of the cofactor (*8*). The *re*-face specificity of proton transfer in bsDAAT and eBCAT have been further confirmed by X-ray crystallographic studies of these enzymes (*9–11*). Because the configuration between the cofactor and catalytic base at the active site is considered to reflect the stereospecificity of

[1] This study was supported by Grants-in-Aid for Scientific Research [No. 11133254 (Priority Areas)] from the Ministry of Education, Science, Sports and Culture of Japan, and by a Research Grant from the Japan Society for the Promotion of Science (Research for the Future). Coordinates for eADCL have been deposited in the RSCB Protein Data Bank as entry 1ET0.

[2] These authors contributed equally to the work

[3] To whom correspondence should be addressed. Phone: +81-6-6605-2557, Fax +81-6-6605-3131, E-mail: hirotsu@sci.osaka-cu.ac.jp

[4] Present address: Laboratory of Biochemistry and Genetics, NIDDK, National Institutes of Health, Bethesda, USA.

Abbreviations: PLP, pyridoxal 5′-phosphate; ADC, 4-amino-4-deoxychorismate; ADCL, 4-amino-4-deoxychorismate lyase; eADCL, *Escherichia coli* ADCL; BCAT, branched-chain amino acid aminotransferase; eBCAT, *Escherichia coli* BCAT; DAAT, D-amino acid aminotransferase, bsDAAT, *Bacillus* species YM-1 DAAT; MIR, multiple isomorphous replacement; r.m.s., root mean square; Tyr109*, the asterisk (*) after the residue number indicates a residue from another subunit of the dimer unit.

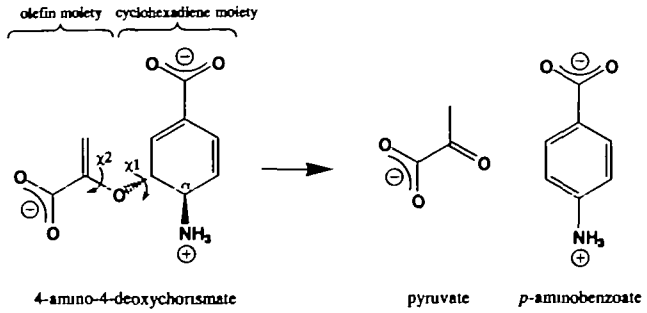

Scheme 1. **Reaction catalyzed by ADCL.**

the hydrogen transfer, ADCL, DAAT, and BCAT are expected to have a common structure different from those of the other fold types of PLP-dependent enzymes.

In contrast to bsDAAT (*12*) and eBCAT (*13*, *14*) that catalyze transamination, ADCL catalyzes a unique reaction, the elimination of pyruvate from ADC with aromatization of the ring. Structure determination of ADCL should help in understanding the structure–function relationship of not only ADCL but also the PLP-dependent enzymes. X-ray crystallographic studies of PLP-dependent lyases have been carried out on tyrosine phenol-lyase (*15*), tryptophan indole-lyase (*16*) and cystathionine β-lyase (*17*), all of which belong to fold type I and have *si*-face specificity of proton transfer. Thus, this is the first structure elucidation of a PLP-dependent lyase belonging to fold type IV and having *re*-face specificity. Here we report the results of an X-ray crystallographic study of eADCL in the unliganded form at 2.2 Å and propose a reaction mechanism based on the model structure for the ADC-PLP external aldimine intermediate.

MATERIALS AND METHODS

Protein Expression, Purification, and Crystallization—The structural gene of eADCL was inserted between the *Eco*RI and *Hin*dIII restriction sites of plasmid pKK223-3. *E. coli* JM109 was transformed with the resultant plasmid, pADCL. The enzyme was purified by ammonium sulfate fractionation and three-step column chromatography, first on a DEAE-Toyopearl column (TOSOH) with a linear gradient from 0 to 0.3 M KCl, followed by a Butyl Toyopearl column (TOSOH) using a linear gradient of saturated ammonium sulfate (30 to 0%), and finally by a MonoQ column (Pharmacia) with a linear gradient from 0.1 to 0.5 M KCl. Selenomethionyl ADCL was prepared by overexpressing pADCL in DL41(metA-) cells grown in the presence of selenomethionine. The selenomethionyl protein was purified and crystallized similar to the wild type one.

Preliminary crystallization conditions for the PLP-type eADCL in the unliganded form were determined using the sparse-matrix method (*18*) along with the hanging-drop vapor-diffusion method (*19*). Several crystal forms were obtained and one of the most promising crystallization conditions was optimized. A droplet of 5 μl protein solution (5 mg/ml protein, 0.1 mM PLP, and 20 mM potassium phosphate buffer, pH 6.5) was mixed with an equal volume of reservoir solution (17% polyethylene glycol 6000, 17% 2-propanol, 100 mM citrate buffer, pH 6.5) and equilibrated against 400 μl of reservoir solution at 293 K. After a few days, small yellow prisms started to grow and were used as seeds for growing large crystals under the same hanging drop conditions. Within 2 weeks, crystals had grown to dimensions of about 0.2 × 0.2 × 0.8 mm.

Data Collection—An X-ray diffraction data set for a native crystal was collected to 2.2 Å resolution at 287 K on the BL6A station at the Photon Factory, KEK (Tsukuba), using an X-ray beam of wavelength 1.00 Å and Fuji imaging plates with a screenless Weissenberg camera (*20*). The space group is $P2_12_12$ with cell dimensions of a = 40.5, b = 73.9, and c = 83.7 Å. There is one subunit in the asymmetric unit, and approximately 42% of the crystal volume is occupied by solvent. The data sets for crystals soaked in 1 mM methylmercury chloride and 1 mM *p*-chloromercuribenzoate, and a selenomethionyl protein crystal were collected to 2.5, 4.0 and 2.5 Å resolution, respectively, at 293 K with a Rigaku R-AXIS IIc imaging plate detector using monochromated Cu $K\alpha$ radiation (40 kV, 100 mA). All data were processed and scaled using the programs DENZO and SCALEPACK (*21*) (Table I).

Structure Determination—The primary sequence of eADCL is 22 and 23% identical to those of eBCAT and bsDAAT, respectively (*7*). The molecular replacement method was used to solve the structure of ADCL using the known structures of bsDAAT and eBCAT as the search models. One marked solution was obtained for both models, and the electron density maps calculated from either model gave the assembly of β-strands in the protein core region. However, the assembly could not be extended to the overall folding of the protein. Therefore, the structure of ADCL was solved by the MIR method using three isomorphous data sets. Data scaling and map calculations were performed with the CCP4 program suite (*22*). The difference Patterson map calculations for methylmercury chloride using the data from 15.0–3.5 Å resolution and *p*-chloromercuribenzoate using the data from 15.0–4.0 Å resolution allowed a clear interpretation of the two and one mercury sites, respectively. A common origin for these derivatives was determined by calculating the difference Fourier summation for *p*-chloromercuribenzoate based on the phases calculated by the mercury sites of methylmercury chloride. Two other minor mercury sites of methylmercury chloride derivative were determined from the difference Fourier maps based on the phase calculated using the major mercury sites. The positions of six selenium sites out of seven in the selenomethyonyl ADCL were determined from the difference Fourier maps based on mercury phasing. Refinement of the heavy atom parameters and calculation of the initial phases were performed with the program MLPHARE (*22*). The resulting MIR map has a mean figure-of-merit of 0.46 at a resolution of 15 to 3.0 Å. The map was significantly improved by the process of solvent flattening (*23*) and histogram matching (*24*) using the program DM (*22*). The mean figure-of-merit reached 0.78 with the same resolution range.

Although, at this stage, the quality of the electron density map was not good enough to build an entire molecule, the β-sheets in the core region were located at the same position as that of the assembly of β-strands observed in the map calculated on the basis of molecular replacement. Moreover, the selenium sites determined by the difference Fourier map coincided with the positions with methionines expected for the models determined by molecular replacement. Thus, a partial model consisting of 127 out of the 269

residues and PLP was built using the electron density of the core region with the program O (*25*). The phases calculated from this model were combined with the MIR phases by the program SIGMAA (*26*). The mean figure-of-merit reached 0.78 at a resolution of 15–3.0 Å. Two cycles of this procedure allowed us to build a model consisting of 207 out of the 269 residues. The structure was refined by simulated annealing using the program X-PLOR (*27, 28*) using X-ray data from 8.0–3.0 Å resolution. The structure including the PLP molecule was scrutinized by successively omitting 10 residue segments of the model from the phasing calculation and inspecting the map to give an additional 47 residues. Refinement by simulated annealing and rebuilding was alternated until no further improvements in structure and statistics were apparent with an R_{factor} of 27.2% and R_{free} of 38.7%. The resolution was progressively increased to 2.2 Å, and after several rounds of refinement and manual rebuilding, the R_{factor} and R_{free} values were reduced to 24.6 and 32.3%, respectively. Water molecules were picked up on the basis of peak heights and distance criteria from the difference map. Water molecules whose thermal factors were above 49 Å^2 (maximum thermal factor of the main chain) after refinement were removed from the list. Further model building and refinement cycles resulted in an R_{factor} of 20.6% and R_{free} of 27.9%, using 11,893 reflections [$Fo > 2\sigma(Fo)$] between 8.0 and 2.2 Å resolution (Table I). During the last step of refinement, unambiguous water molecules were added even those with a temperature factor higher than 49 Å^2.

TABLE I **Data collection, MIR, and refinement statistics.**

Crystal	Native	Se-Met	CH_3HgCl	PCMB[e]
Diffraction data				
Resolution (Å)	2 2	2.5	2 5	4.0
No of reflections				
Unique	12,330	8,849	5,608	2,152
Observed	88,073	—	—	—
Completeness (%)	92 2 (85.0)[d]	98 3	85 7	90 8
R_{merge}[a] (%)	7 2 (13.5)[d]	5.8	9 5	11.1
MIR				
R_{diff}[b] (%)		11.2	15 7	14 4
Phasing power[c]		1.05	1 06	0 91
No. of sites		6	4	1
Refinement				
Resolution limits (Å)	8.0–2.2			
R_{factor} (%)	20 6 (25.1)[d]			
R_{free} (%)	27.9 (27.5)[d]			
Deviations				
Bond lengths (Å)	0.008			
Bond angles (deg)	1.4			
Mean *B* factors				
Main chain atoms (Å^2)	15.8			
Side chain atoms (Å^2)	19.1			
Cofactor atoms (Å^2)	11.8			
Water atoms (Å^2)	36 6			

[a] $R_{merge} = \Sigma_{hkl}\Sigma_i|I_{hkl,i}-\langle I_{hkl}\rangle|/\Sigma_{hkl}\Sigma_i I_{hkl,i}$, where I = observed intensity and $\langle I\rangle$ = average intensity for multiple measurements. [b] $R_{diff} = \Sigma||F_{PH}|-|F_P||/\Sigma|F_P|$, where $|F_{PH}|$ and $|F_P|$ are the derivative and native structure-factor amplitudes, respectively. [c] Phasing power is the ratio of the root mean square (r.m.s.) of the heavy atom scattering amplitude and the lack of closure error. [d] The values in parentheses are for the highest resolution shell (2.3–2.2 Å). [e] *p*-chloromercuribenzoate.

Quality of the Structure—The refined model of eADCL contains 1964 non-hydrogen protein atoms and a covalently bound molecule of PLP. Additionally, 126 water molecules were included (Table I). Almost all amino acid residues were found to have good electron densities in the final $(2F_{obs}-F_{calc})$, α_{calc} map. However, this model lacks the following 15 residues due to poor electron density: Tyr126 to Gly137 (the residues connecting two domains) and Arg290 to Asn292 (C-terminal residues) (Fig. 1). The average thermal factors of the main chain atoms (N, Cα, C, and O) are 15.8 Å^2. Analysis of the stereochemistry with PROCHECK (*29*) showed that all the main-chain atoms except Gln90 fall within the generously allowed regions of the Ramachandran plot with 198 residues in the most favored region and 25 in the additionally allowed region. On the basis of the electron density maps, it is confirmed that the conformation of Gln90 is correct. Two proline residues (Pro116 and Pro260) were found in the *cis*-conformation.

Modeling of eADCL in Complex with ADC—The non-hydrogen atoms of the active site residues of the unliganded eBCAT are superimposed on those of the complex form with 2-methylleucine (an external aldimine model) by least-square fitting with r.m.s. deviations of 0.38 Å, except for Arg40 and Tyr107* (*11, 30*). Similarly, the corresponding atoms of the unliganded bsDAAT are superimposed on those of the reconstructed form by *N*-(5′-phosphopyridoxyl)-D-alanine (the reduced analogue of the external aldimine) with r.m.s. deviations of 0.23 Å, except for His86 and Tyr88 (*9, 10*). Thus, upon binding of a substrate, the active site residues do not exhibit any appreciable change in their side chain conformations except for a few residues, implying that the active site structure of the unliganded eADCL belonging to fold type IV together with eBCAT and bsDAAT may be used as an active site model of the liganded one. On the formation of the external aldimine form, the cofactor PLP in eBCAT or bsDAAT rotates toward the solvent side to make a Schiff base linkage with the substrate. The substrate-PLP Schiff base bound to the active site of eBCAT was observed to have a very similar location and conformation as that of bsDAAT (*10, 30*), suggesting that the ADC-PLP external aldimine (Schiff base) may have the same orientation as those observed in the liganded eBCAT and bsDAAT, and could be modeled into the active site of the unliganded eADCL.

The external aldimine model of eADCL was constructed as follows. (i) The ADC-PLP Schiff base was positioned at the active site of the unliganded eADCL so as to give the same orientation as that of the 2-methylleucine-PLP Schiff base in eBCAT (*30*). (ii) The cyclohexadiene moiety of ADC was positioned by directing an α-proton toward the protein side and by assuming that the α-carbon and two carbon atoms adjacent to the α-carbon in the cyclohexadiene ring correspond to Cα, and Cβ, and an α-carboxylate carbon of the substrate analogue (2-methylleucine) in the external aldimine form of eBCAT. (iii) The olefin moiety of ADC has two freedoms of rotation around two C-O bonds of an ether linkage. The torsional angles around the two C-O bonds were changed stepwise to determine the most favorable interaction between the olefin moiety and the active site residues. The olefin moiety was fixed at the position where the carboxylate of the olefin moiety forms a salt bridge with Lys97. (iv) The model structure thus obtained was optimized using an energy-minimization method with the pro-

```
                  10        20        30             40        50        60             70
bsDAAT -----GYTLWNDQIVKDEEVKIDKEDRGYQFGDGVYEVVKVYN----GEMFTVNEHIDRLYASAEKIRITIPYT-----KDKFH
             <b1>  <b2>           <a1->  <--b3--->     <b4> <-----a2----->              <----
               10        20        30        40        50        60        70
eBCAT  TTKKADYIWFNGEMVRWEDAKVHVMSHALHYGTSVFEGIRCYDSHKGPVVFRHREHMQRLHDSAKIYRFPVSQS-----IDELM
             <b1>  <b2>   <b0>   <a1-> <b3>  <-b4->  <b5-> <-----a2------>             <----
eADCL  ------MFLINGHKQ----ESLAVSDRATQFGDGCFTTARVID----GKVSLLSAHIQRLQDACQRLMISCD-F-----WPQLE
             <b1> <b2>    <b0>   <a1->  <--b3--->     <b5> <-----a2----->             <----
vhADCL ------MFWVNGLPQ----THVPLGDRSFQYGDGCFSTIKTKK----GQLEHWQAHVERMEACLTTIQIPFP-D-----WRTVL
bsADCL ------MIYVNGRYMEEKDAVLSPFDHGFLYGIGVFETFRLYE----GCPFLLDWHIERLERALKDLQIEYTVSK-HEILEMLD
aaADCL ------------------------MNRTLQYGEGLFETI-LWE----GENYKLRKHYERLKNSANFFGFPYPSYK------EFL
CONS                          l         G G f t         g       H qRl

               80        90         100       110       120        130       140
bsDAAT QLLHELVEKNELNTGHIYFQVT-RGT-SPRAHQFPENTVKPVIIGYTKENPRP--LENLEKGVKATFVEDIRWL----RCDIKS
       --a3----->    <--b5-->                    <--b6-->      <-a4-> <-b7-->
      80        90        100        110       120       130       140       150       160
eBCAT  EACRDVIRKNNLTSAYIRPLIF-VGD-VGMGVNPPA-GYSTDVIIAAFPWGAYLGAEALEQGIDAMVSSWNRAAPNTIPTAAKA
       --a3----->    <--b6-->                    <-b7-->             <b8->
eADCL  QEMKTLAAEQQ--NGVLKVVIS-RGS-GGRGYSTLN-SGPATRILSVTAYPAHYDRLRNEG-ITLALSPVRLGRNP-HLAGIKH
       --a3----->    <--b5-->                    <-b6-->              <b7>
vhADCL DWAMSATLKDE--SAGIKIHIS-RGC-GGRGYSPSG-VEGPVVTISNFSFPAHYLAWQERG-VQLGVCETRLGIQP-LLAGHKH
bsADCL KLLKLNDIKDG--NARVRLNIS-AGI-SDKGFVAQT-YDKPTVLCFVNQLKPESLPLQKEG----KVLSIRRNTPE-GSFRLKS
aaADCL GEIQEATKGKK--GLYVKFLVAYRGS-DYYGDLPEE-YEIKVYTRELPKIPKSVKLC---------ISEVRKHSKN-PLIYHKT
CONS                    lk   s  G                                                        K

         150       160       170       180              190       200       210       220
bsDAAT LN-LLGAVLAKQEAHEKGCYEAILHR-NNTVTEGSSSNVFGIKDG-------ILYTHPANNMILKGITRDVVIACANEINMPV
           <----a5---->    <-b8->   <b9->   <b10->        <b11>          <----a6---->    <
             170       180       190       200              210       220       230
eBCAT  GGNYLSSLLVGSEARRHGYQEGIALDVNGYISEGAGENLFEVKDG-------VLFTPPFTSSALPGITRDAIIKLAKELGIEV
          <----a4----->    <b9->     <b10>  <b11>          <b12>          <----a5---->   <-
eADCL  LN-RLEQVLIRSHLEQTNADEALVLDSEGWVTECCAANLFWRKGN-------VVYTPRLDQAGVNGIMRQFCIRLLAQSSYQL
           <---a4--->      <b8->     <b9>   <b10->         <b11>          <----a5---->   <-
vhADCL NN-RIEQVLAKAEIDGTEFADAVTLNVQNHVIETTMANLFWVKDE-------KVFTPGLCLSGVAGVMRRKVLEYLQSEGYSV
bsADCL HH-YLNNMYAKREIGNDPRVEGIFLTEDGAVAEGIISNVFWRKGR-------CIYTPSLDTGILDGVTRRFIIENAKDIGLEL
aaADCL TS-FFLNTYTKREAKAKGFYDAVILNEKEYITETSSANLLLYKDG-------RFYTPARESGLLWGTTLDILCEEL-----EV
CONS             r         e l l     v E    nl   k            Tp      v G

               230       240       250       260       270       280
bsDAAT KEIPFTTHEALKMDELFVTSTTSEITPVIEIDGKLIRDGKV-GEWTRKLQKQFETKIPKPLHI----------
       b12>  <-a7->  <b13->    <b14><b15 b16>      <---a8---->
        240       250       260       270       280       290       300
eBCAT  REQVLSRESLYLADEVFMSGTAAEITPVRSVDGIQVGEGRC-GPVTKRIQQAFFGLFTGETEDKWGWLDQVNQ
       b13>    <a6>  <b14->    <b15><b16 b17>      <---a7---->             b18
eADCL  VEVQASLEESLQADEMVICNALMPVMPVCACGDVSFSS----ATLYEYLAPLCERPN----------------
       b12>  <a6>    <b13->    <b14><b15>          <---a7--->
vhADCL QVADFTLTDLLDADEVWMCNSLLGVAPVSGISAPENKIDFPIGKLTRRLQGNLNT------------------
bsADCL KTGRYELEALLTADEAWMTNSVLEIIPFTKIEEVNYGSQS--GEATSALQLLYKKEIKNMIHEKGGRAWRSTQ
aaADCL REEKIKLDFLSSCESVFILNSLLLVVPVSEIEGKVFKVD---EELTRELREALKKLSNK--------------
CONS          l      d   i n l                          l
```

Fig 1 **Alignments of bsDAAT, eBCAT, and four ADCLs with secondary structures.** α-Helices are denoted as a1–a8 and β-strands as b0–b17. bsDAAT and eBCAT are from *Bacillus* sp YM-1 and *E. coli*, respectively eADCL, vhADCL, bsADCL, and aaADCL are from *E. coli*, *Vibrio harveyi*, *Bacillus subtilis*, and *Aquifex aeolicus*, respectively In the consensus sequence, capital letters show conserved residues, and small letters denote homologous residues in ADCLs The numbering of the primary sequence of bsDAAT is from Ref. *9*.

gram XPLOR (*31*) to lower the energy of the model structure by 3.8 kcal mol^{-1}. The protein atoms were restrained by harmonic potentials (20 kcal/mol Å² for Cα atoms, 3 kcal/mol Å² for all others) as described by Storici *et al.* (*32*).

RESULTS AND DISCUSSION

Primary Structure—The primary sequence of eADCL was aligned *versus* those of bsDAAT and eBCAT based on the three-dimensional structures. The details of the procedure was previously described (*33*). Sequence alignment of eADCL with other ADCLs was performed with the program CLUSTAL W (*34*). As a result of these alignments (Fig. 1), the sequence identities of eADCL with respect to bsDAAT, eBCAT, *Vibrio harveyi* ADCL (*35*), *Bacillus subtilis* ADCL (*36*), and *Aquifex aeolicus* ADCL (pir:H70438) are 21, 20, 35, 26, and 20%, respectively. *Helicobacter pylori* ADCL (pir:C64593) is omitted from the alignments because the sequence identity with that of eADCL is too low (<10%). The 269 amino acid residues of eADCL are numbered from Met7 to Asn292 according to the sequence of eBCAT (*13*).

Overall Structure—The eADCL is folded into a dimeric form with a crystallographic two-fold axis, and each subunit is composed of 269 amino acid residues with a subunit molecular weight of 29,715 and PLP. The overall structure of eADCL is shown in Fig. 2. The Cα atoms of eADCL were superimposed against those of bsDAAT and eBCAT by a least-squares fitting with r.m.s. deviation of 1.93 Å for 92.9% structurally equivalent Cα atoms and 2.10 Å (94.4%), respectively. The subunit structure of eADCL is shown with secondary structure assignments by the pro-

gram DSSP (*37*) in Fig. 3. The arrangement of the α-helices and β-sheets of eADCL as a whole is similar to those of bsDAAT and eBCAT of fold type IV (Fig. 1), indicating that among these molecules the secondary and overall structures of the enzymes are conserved.

The subunit of eADCL is divided into one small domain comprising the N-terminus to Ala125 and one large domain comprising Ile139 to the C-terminus. The interdomain loop connecting the small and large domains (Tyr126–Gly137) was disordered in the unliganded form of eADCL, and could not be modeled. Also, in eBCAT, the corresponding interdomain loop in the unliganded form is disordered.

The N-terminal small domain is an α/β structure with an open β-sheet structure. The six antiparallel β-strands designated as β2, β1, β6, β5, β3, and β4 form a twisted β-sheet structure as a central core surrounded by two α-helices (α2 and α3) from the surface side of the protein and a short α-helix (α1) around the twofold axis from the interior side (Figs. 1 and 3). The C-terminal large domain is also an α/β structure with a pseudo β-barrel structure. The β-sheet comprising four strands designated as β9, β8, β7, and β15 (all parallel except for β9) and that comprising five strands designated as β12, β11, β10, β13, and β14 (all antiparallel except for β12) form a pseudo β-barrel surrounded by three

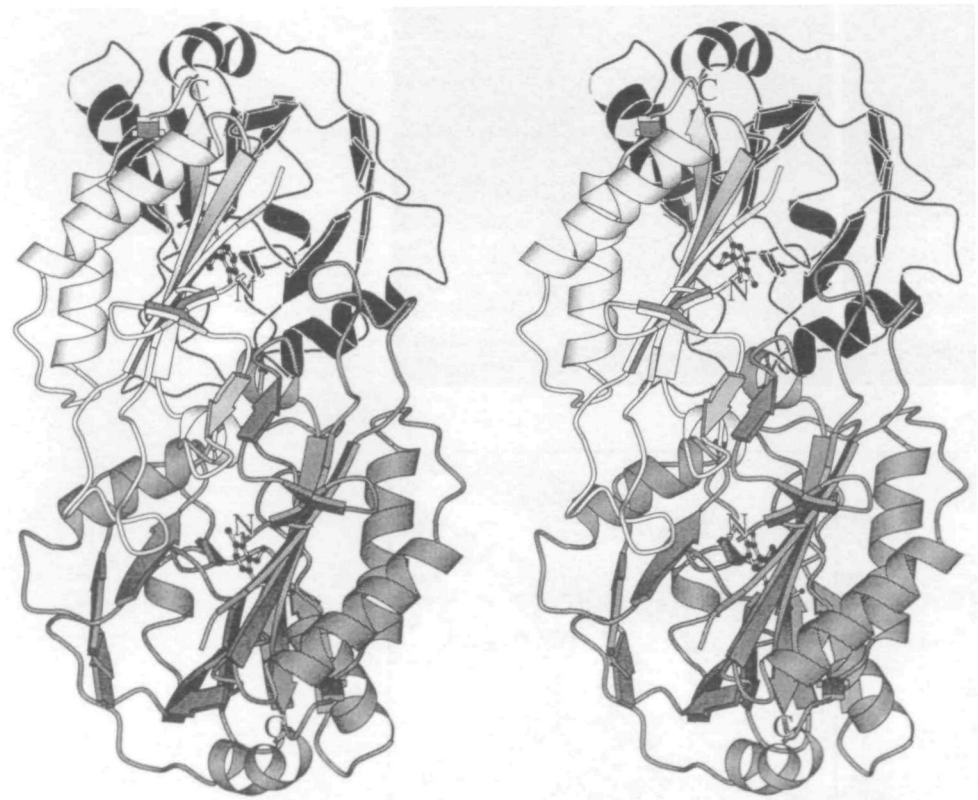

Fig 2 **Cα ribbon tracing of the unliganded eADCL in the PLP-form viewed down the molecular 2-fold axis.** One subunit is represented by the shaded ribbon, and the small and large domains of the other subunit by the lightly shaded and full ribbons, respectively Cofactor PLP, shown by the ball-and-stick model, is bound to the active site pocket, which is located at the domain interface. Two loops of the small domain of the other subunit approach the cofactor PLP

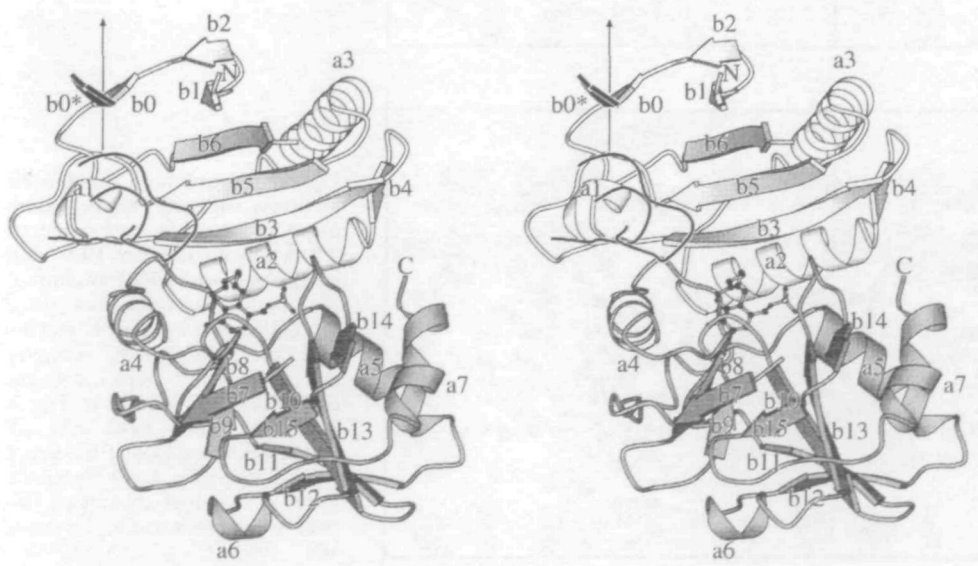

Fig 3 **Stereoview of the subunit structure in the unliganded form with secondary structure assignments.** α-Helices and β-strands are denoted as a1–a3 and b0–b6 in the small domain, and a4–a7 and b7–b15 in the large domain, respectively. The lightly and heavily shaded ribbons represent the small and large domains, respectively The β-strand (b0*) of the other subunit related by a molecular twofold axis is shown by the full ribbon. Two loops (black) of the other subunit shown on the upper left of the figure participate in the formation of the active site.

α-helices (α5, α6, and α7) from the surface side of the protein and an α-helix (α4) from the interior side

The β-strand (β0) and that from the other subunit related by the twofold axis (β0* shown in Fig. 3) form an inter-subunit anti-parallel β-sheet. The α-helix (α1) and the loop between the β-strands (β5 and β6) are also located around the molecular twofold axis participating in the formation of the subunit interface.

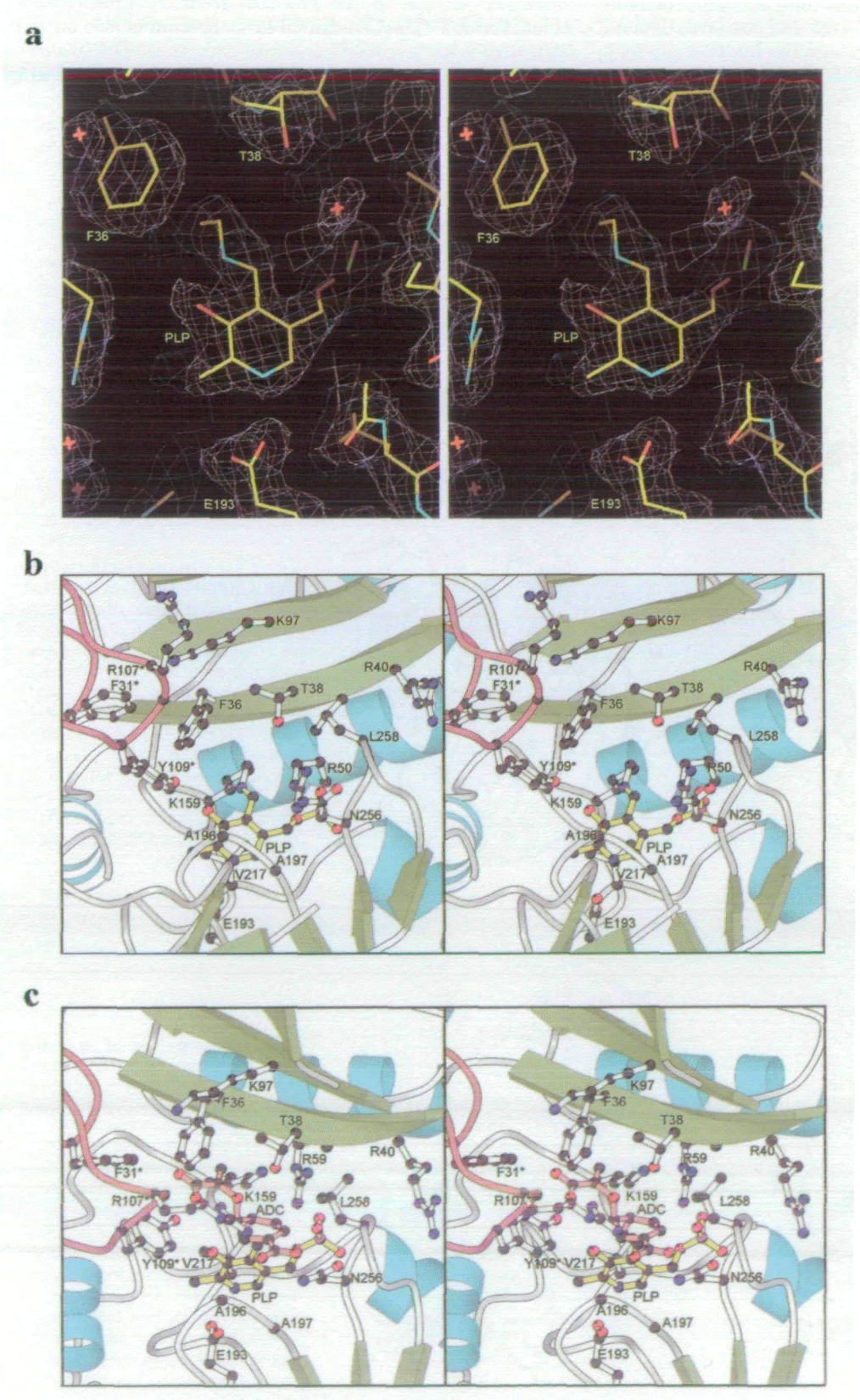

Fig 4 **Stereoview of the 2*Fo–Fc* electron density map calculated using data between 8.0–2.2 Å resolution for PLP and residues close to PLP (a, top).** A close-up view of the active site of the unliganded eADCL (b, middle) and the eADCL-ADC complex model (c, bottom) from nearly the same direction as that in Fig. 3 PLP (pale yellow), ADC (pale red) and selected residues of the active site are shown for clarity. Two loops (pink) of the other subunit participate in the formation of the active site.

The Active Site Structure of the Unliganded eADCL—The active site cleft of the enzyme is located at the domain and subunit interface. The active site comprises the residues from both domains of one subunit and the small domain (two loops shown in Fig. 3) of the other subunit of the dimer unit. The 2*Fo–Fc* electron density map for PLP and the residues around it is shown in Fig. 4a. The structure and hydrogen bonding scheme of the active site are shown in Figs. 4b and 5a, respectively.

PLP binds to the pocket by forming an internal aldimine bond (Schiff base linkage) with the catalytic residue Lys159 and by extensive noncovalent interactions with the residues of the active site. The imine nitrogen of the internal aldimine bond is displaced by 0.65 Å from the pyridine ring of PLP with the dihedral angle of C3-C4-C4′-N = –34°, and makes a hydrogen bond with O3′ of PLP. PLP is sandwiched between the main chain of Ala196-Ala197 and the side chain of Val217 from above and below Glu193 forms an ion pair with the protonated nitrogen atom of the pyridine ring of PLP, and is considered to strengthen the electron withdrawing effect of the pyridine ring of PLP as an electron sink, as has been observed for enzymes of fold types I and IV (*38–40*). Tyr109* is hydrogen bonded to the O3′ of PLP to regulate the electronic state of PLP (*41*, *42*) Residue 109* is Val in eBCAT (*11*) and His in bsDAAT (*9*, *10*), and Tyr164 and a water molecule take the place of Tyr109*, respectively. Some ADCLs in Fig. 1 do not have Tyr109, but have a Tyr164 as in eBCAT. The phosphate group of PLP is involved in seven hydrogen bonds and acts as an anchor to fix the cofactor to the active site. The negative charge of the phosphate group is well balanced with the positive charge of Arg59 and the dipole of the α-helix (α5), whose N-terminus is close to the phosphate group.

The PLP-dependent enzymes have *si*-face specificity of proton transfer with respect to the C4′ of the cofactor except for enzymes of fold type IV. The *re*-face specificity of the proton shuttle was first clarified for bsDAAT and eBCAT by hydrogen transfer experiments (*8*), and further confirmed by X-ray crystallographic studies of these enzymes. eADCL was then proposed to have *re*-face specificity (*43*) An X-ray study of eADCL showed that PLP has the same orientation toward the protein as that found in bsDAAT or eBCAT (*9*, *11*), and rotates by 180° compared with other PLP-dependent enzymes (*38*). The *re*-face of the PLP-ring faces the protein side, and the catalytic residue Lys159 transfers protons on the *re*-face of PLP. Thus, the *re*-face specificity of eADCL was unambiguously determined.

The bottom of the active site pocket consists of Phe36, Arg59, Lys159, Arg164, Glu193, Val217, Ile220, and Met221. The side or wall of the active site is made up of Thr37, Thr38, Arg40, Val95, Lys97, Ala196, Asn256,

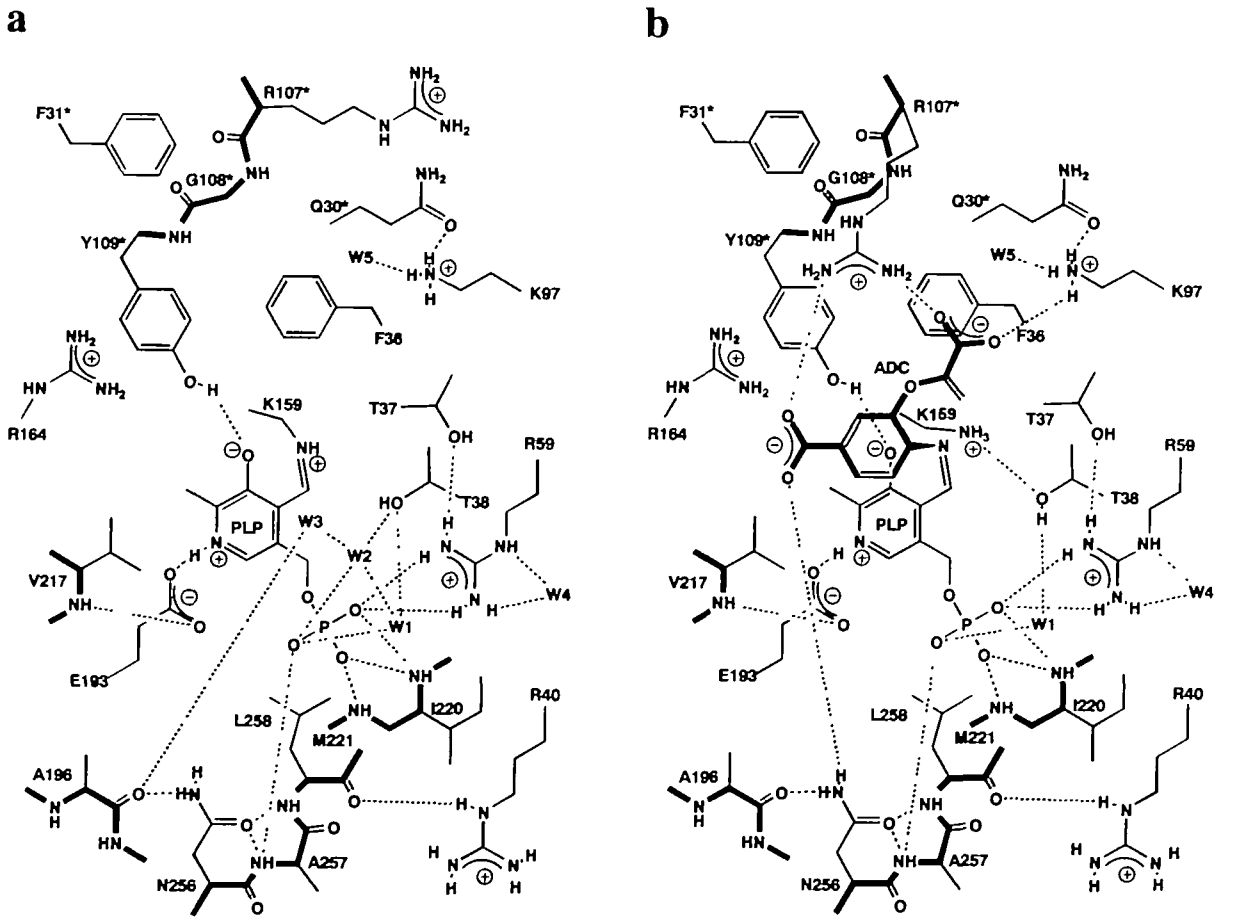

Fig. 5. **Schematic diagram showing hydrogen bond and salt bridge interactions of the active site residues in the unliganded eADCL (a, left) and the eADCL-ADC complex model (b, right).** Putative interactions are shown by dotted lines if the acceptor and donor are less than 3 5 Å apart.

Ala257, Leu258, Phe31*, Arg107*, Gly108*, and Tyr109*. Three water molecules (W1, W2, and W3) are located in the vicinity of the PLP ring, and are involved in the formation of the hydrogen bonding network as shown in Fig. 5a. When the active site residues of eADCL are compared with those of eBCAT (*11*) and bsDAAT (*9*), the only residues conserved are Arg59, Lys159, and Glu193, all in the bottom of the active site, and conserved in all known ADCLs. Arg59 is the key residue fixing the phosphate group of PLP, and Lys159 and Glu193 are catalytically-critical residues as described above. None of the residues from the wall of the active site are conserved. In spite of the poor conservation of the active site residues, the main chain atoms of the active site residues of eADCL fit those in eBCAT and bsDAAT with r.m.s. deviations of 0.89 and 0.78 Å, except for the residues 258 and 107*, respectively. The eADCL, eBCAT, and bsDAAT enzymes belonging to fold type IV are divergently evolved from the same ancestor to have different substrate and reaction specificities by replacing most of the active site residues except for the critical Arg59, Lys159, and Glu193 residues for enzyme functions, but by maintaining the main chain folding of the active site. This result indicates that in principle PLP-dependent enzymes with quite different substrate specificities and/or different reaction specificities can be designed by protein engineering starting from fold type IV enzymes, but in practice, the engineering is quite difficult since too many residues must be rationally replaced.

The primary sequences of ADCLs depicted in Fig. 1 show that in addition to Arg59, Lys159, Glu193, and Val217, the roles of which have already been described, Phe36, Thr38, Lys or Arg97, Asn256, Leu or Val258, and Arg or Lys107* are conserved in almost all ADCLs as the active site residues. These residues are possibly concerned with substrate recognition or the catalytic action of the enzyme.

Interestingly, upon binding of a substrate analogue, the interdomain loop of eBCAT shows its ordered structure to close the active site and shield the analogue from the solvent region, and plays important roles in substrate recognition (*30*). Similarly, the disordered interdomain loop of eADCL might be ordered to close the active site upon binding of a substrate, but the exact behavior of the loop can not be seen until the structure of eADCL in complex with a substrate or inhibitor is determined.

The Active Site Structure of the eADCL-ADC Complex Model—A model of eADCL in complex with the substrate

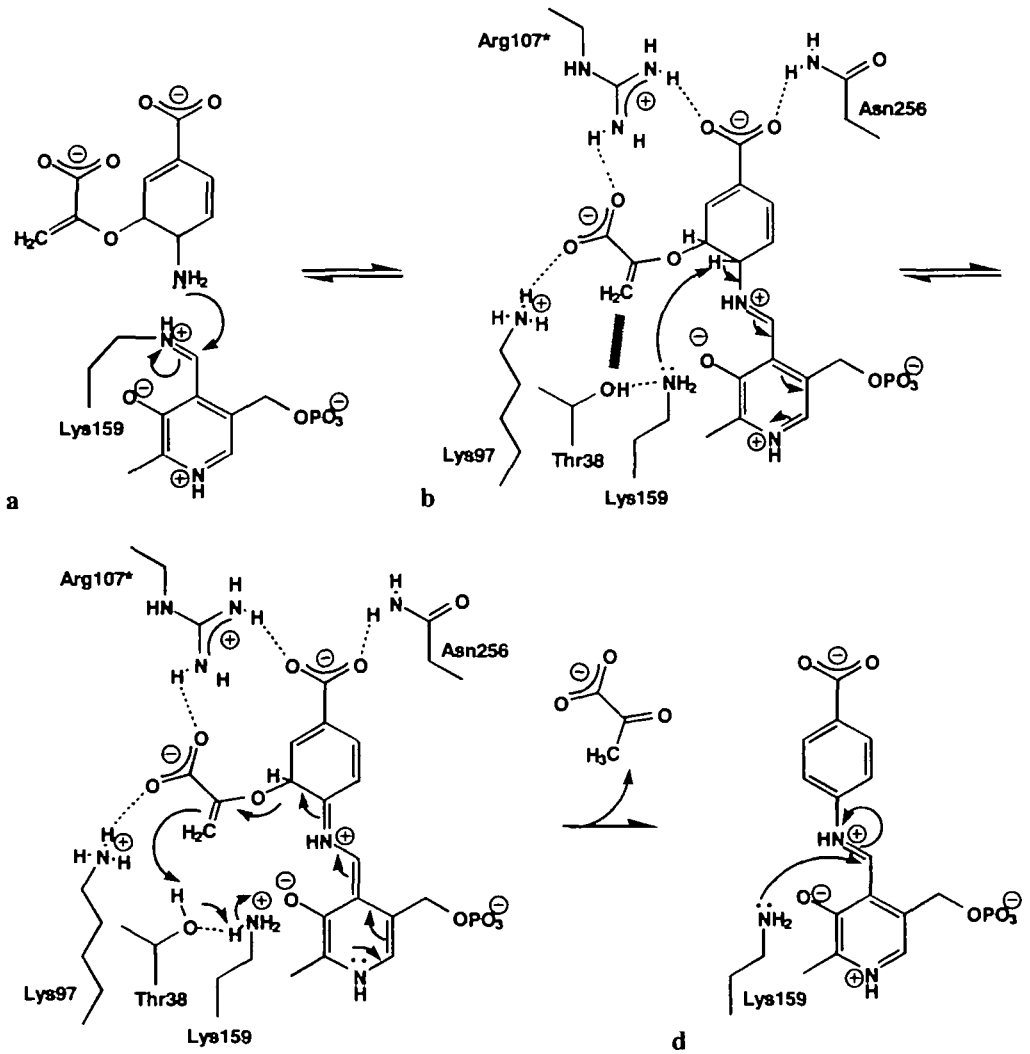

Fig. 6. The proposed reaction mechanism of eADCL with ADC to produce *p*-aminobenzoate and pyruvate.

ADC (the external aldimine model) was constructed and the energy minimized with X-PLOR (*31*) as described in "MATERIALS AND METHODS". The active site structure and hydrogen bonding scheme of the final model are displayed in Figs. 4c and 5b, respectively. On binding of ADC, two water molecules, W2 and W3, are expelled from the active site of the unliganded eADCL, and PLP forms a new Schiff base with ADC to release Lys159 with a neutral amino group, which is hydrogen bonded to the hydroxy group of Thr38. All the residues of the active site in the complex model have essentially the same positions as those in the unliganded eADCL except for Arg107 and Lys159, whose side chains move by more than 1 Å. Almost all the hydrogen bonds found in the active site of the unliganded eADCL are thus maintained in the complex model. Glu193 makes a salt bridge with the protonated nitrogen atom of the pyridine ring of PLP, Tyr109* is hydrogen bonded to the O3′ of PLP, and the phosphate group of PLP is fixed to the active site by hydrogen bonds.

The amino group of Asn256 is hydrogen bonded to the carboxylate of the cyclohexadiene moiety of the bound ADC. Arg107* changes its side chain direction toward the active site to form salt bridges with two carboxylates of ADC. The directional change in Arg107* is reminiscent of the behavior of Arg292* in aspartate aminotransferases upon the binding of a substrate (*44–47*). The protonated amino group of Lys97 interacts with the carboxylate of the olefin moiety The side chain of Leu258 makes van der Waals contact with the cyclohexadiene moiety of ADC.

Mechanistic Implications—A possible reaction mechanism of eADCL with ADC to give *p*-aminobenzoate and pyruvate is shown in Fig. 6 based on the stereochemical consideration of the external aldimine model described above and the proposed mechanism (*7*). The eADCL binds ADC to give a Michaelis complex (**a** in Fig. 6). ADC is reasonably postulated to occupy the same position as that of the ADC moiety in the external aldimine form, since the X-ray structures of the aspartate aminotransferases and eBCAT show that substrate analogues in Michaelis complexes do not change their locations during the formation of the external aldimines (*30*, *44–46*). The amino group of ADC is directed toward the PLP-Lys159 Schiff base linkage, and the C4′ of PLP undergoes nucleophilic attack by the amino group of ADC. Through the tetrahedral intermediate, a PLP-ADC Schiff base (external aldimine) is formed between PLP and ADC to release Lys159 (**b**). The neutral amino group of Lys159 makes a hydrogen bond with Thr38, which will decrease the free energy level of the external aldimine form of the enzyme. The OH group of Thr38 makes van der Waals contact with the methylene group of ADC. The α-carbon of the substrate is activated by the protonated Schiff base and the protonated pyridine ring. The α-proton of the substrate is nearly perpendicular to the plane defined by the Schiff base, pyridine ring and α-carbon, and is directed toward Lys159, which is the only base able to abstract the α-proton. Thus, good conditions for α-proton elimination are achieved to give a quinonoid intermediate (**b** and **c**). The quinonoid intermediate is stabilized by the delocalization of the cofactor-substrate π-system and the hydrogen bond between N1-H of the cofactor ring and Glu193. The electron would migrate toward the substrate from the cofactor in accord with the proton transfer from Thr38 to the olefin moiety of the substrate, resulting in the release of a pyruvate with aromatization of the six-membered ring of the substrate (**c** and **d**). Then, *p*-aminobenzoate will be liberated to recover the starting Schiff base by the reverse of the reaction process from step **a** to step **b**.

The final elucidation of the substrate recognition and reaction mechanism of ADCL awaits the X-ray crystallographic determinations of eADCL in complex with substrate analogues, which are now in progress. The results reported here form the basis for future investigations on the structure-function relationships of eADCL and other related members of fold type IV PLP-dependent enzymes, including studies of the catalytic action by inhibitor binding and site-directed mutagenesis.

We would like to thank Professor Emeritus N. Sakabe (National Laboratory for High Energy Physics), and Drs. N Watanabe, M. Suzuki, and N. Igarashi (High Energy Accelerator Research Organization) for their help in data collection through synchrotron radiation

REFERENCES

1 Green, J M. and Nichols, B P (1991) *p*-Aminobenzoate biosynthesis in *Escherichia coli*. Purification of aminodeoxychorismate lyase and cloning of *pabC J Biol Chem* **266**, 12971–12975
2. Anderson, K.S., Kati, W.M , Ye, Q -Z., Liu, J , Walsh, C T., and Johnson, A.J (1991) Isolation and structure elucidation of the 4-amino-4-deoxychorismate intermediate in the *p*-aminobenzoic acid pathway *J Am. Chem. Soc.* **113**, 3198–3200
3 Teng, C -Y P. and Ganem, B (1984) Shikimate-derived metabolites 13 A key intermediate in the biosynthesis of anthranilate from chorismate *J Am. Chem Soc.* **106**, 2463–2464
4 Teng, C -Y P., Genem, B., Doktor, S.Z , Nichols, B P , Bhanager, R.K., and Vining, L.C (1985) Total synthesis of (±)-4-amino-4-deoxychorismic acid: a key intermediate in the biosynthesis of *p*-aminobenzoic acid and L-(*p*-aminophenyl)alanine. *J Am. Chem Soc.* **107**, 5008–5009
5 Ye, Q.-Z , Liu, J , and Walsh, C.T. (1990) *p*-Aminobenzoate synthesis in *Escherichia coli* purification and characterization of *PabB* as aminodeoxychorismate synthase and enzyme X as aminodeoxychorismate lyase. *Proc. Natl. Acad. Sci USA* **87**, 9391–9595
6 Grishin, N V , Phillips, M.A., and Goldsmith, E J (1995) Modeling of the spatial structure of eukaryotic ornithine decarboxylases. *Protein Sci* **4**, 1291–1304
7 Green, J M , Merkel, W.K., and Nichols, B.P. (1992) Characterization and sequence of *Escherichia coli pabC*, the gene encoding aminodeoxychorismate lyase, a pyridoxal phosphate-containing enzyme. *J. Bacteriol* **174**, 5317–5323
8 Yoshimura, T., Nishimura, K., Ito, J , Esaki, N , Kagamiyama, H , Manning, J M., and Soda, K. (1993) Unique stereospecificity of D-amino acid aminotransferase and branched-chain L-amino acid aminotransferase for C-4′ hydrogen transfer of the coenzyme. *J. Am. Chem. Soc.* **115**, 3897–3900
9. Sugio, S , Petsko, G.A., Manning, J.M , Soda, K., and Ringe, D. (1995) Crystal structure of a D-amino acid aminotransferase· how the protein controls stereoselectivity. *Biochemistry*, **34**, 9661–9669
10. Peisach, D., Chipman, D M., van Ophem, P.W., Manning, J M., and Ringe, D. (1998) Crystallographic study of steps along the reaction pathway of D-amino acid aminotransferase. *Biochemistry* **37**, 4958–4967
11 Okada, K., Hirotsu, K., Sato, M , Hayashi, H., and Kagamiyama, H (1997) Three-dimensional structure of *Escherichia coli* branched-chain amino acid aminotransferase at 2.5 Å resolution. *J. Biochem* **121**, 637–641
12. Tanizawa, K., Asano, S , Masu, Y., Kuramitsu, S., Kagamiyama, H., Tanaka, H., and Soda, K. (1989) The primary structure of thermostable D-amino acid aminotransferase from a thermo-

philic *Bacillus* species and its correlation with L-amino acid aminotransferases. *J. Biol Chem* **264**, 2450–2454
13. Kuramitsu, S, Ogawa, T, Ogawa, H, and Kagamiyama, H. (1985) Branched-chain amino acid aminotransferase of *Escherichia coli* nucleotide sequence of the *ilv*E gene and the deduced amino acid sequence. *J. Biochem.* **97**, 993–999
14. Inoue, K., Kuramitsu, S, Aki, K., Watanabe, Y, Tagaki, T., Nishigai, M., Ikai, A., and Kagamiyama, H (1988) Branched-chain amino acid aminotransferase of *Escherichia coli* overproduction and properties. *J Biochem.* **104**, 777–784
15. Sundararaju, B., Antson, A.A., Phillips, R S, Demidkina, T.V, Barbolina, M V., Gollnick, P, Dodson, G.G, and Wilson, K.S (1997) The crystal structure of *Citrobacter freundii* tyrosine phenol-lyase complexed with 3-(4'-hydroxyphenyl)propionic acid, together with site-directed mutagenesis and kinetic analysis, demonstrates that arginine381 is required for substrate specificity. *Biochemistry* **36**, 6502–6510
16. Isupov, S V, Antson, A.A., Dodson, E.J, Dementieva, I.S, Zakomirdina, L N., Wilson, K.S., Dauter, Z., Lebedev, A.A., and Harutyunyan, E.G (1998) Crystal structure of tryptophanase. *J. Mol Biol* **276**, 603–623
17. Clausen, T., Huber, R, Laber, B., Pohlenz, H-D., and Messerschmidt, A. (1996) Crystal structure of the pyridoxal-5'-phosphate dependent cystathionine β-lyase from *Escherichia coli* at 1 83 Å. *J. Mol Biol* **262**, 202–224
18. Jancarik, J and Kim, S.-H. (1991) Sparse matrix sampling: a screening method for crystallization of proteins. *J. Appl Crystallogr* **24**, 409–411
19 McPherson, A. (1982) *Preparation and Analysis of Protein Crystals*, Wiley, New York
20 Sakabe, N. (1991) X-ray diffraction data collection system for modern protein crystallography with Weissenberg camera and an imaging plate using synchrotron. *Nucl Instr Methods Phys. Res.* **A303**, 448–463
21 Otwinowski, Z (1993) Data collection and processing in *Proceedings of the CCP4 Study Weekend*, pp. 56–62, SERC Daresbury Laboratory, Warrington
22 Collaborative Computational Project Number 4 (1994) The CCP4 suite. programs for protein crystallography *Acta Crystallogr.* **D50**, 760–763
23 Wang, B.-C. (1985) Resolution of phase ambiguity in macromolecular crystallography. *Methods Enzymol.* **115**, 90–112
24 Zhang, K.Y.J. and Main, P. (1990) The use of Sayre's equation with solvent flattening and histogram matching for phase extension and refinement of protein structures. *Acta Crystallogr.* **A46**, 377–381
25 Jones, T.A., Zou, J-Y, Cowan, S.W., and Kjeldgaard, M. (1991) Improved methods for building protein models in electron density maps and the location errors in these models. *Acta Crystallogr.* **A47**, 110–119
26. Read, R.J. (1986) Improved Fourier coefficients for maps using phases from partial structures with errors. *Acta Crystallogr.* **A42**, 140–149
27. Brünger, A.T., Kuriyan, J, and Karplus, M (1987) Crystallographic R factor refinement by molecular dynamics. *Science* **235**, 458–460
28 Brünger, A.T (1991) Simulated annealing in crystallography. *Annu. Rev. Phys. Chem.* **42**, 197–223
29. Laskowski, R.A., MacArthur, M.W., Moss, D S., and Thornton, J.M. (1993) PROCHECK: a program to check the stereochemical quality of protein structures. *J. Appl. Crystallogr* **26**, 283–291
30. Hirotsu, K., Goto, M., Miyahara, I., Hayashi, H., Kagamiyama, H, and Okada, K. (2000) Structure, induced fit and substrate recognition of *E coli* branched-chain amino acid aminotransferase in *Biochemistry and Molecular Biology of Vitamin B6 and PQQ-Dependent Proteins* (Iriarte, A., Kagan, H M., and Martinez-Carrion, M., eds.) Birkhauser Verlag AG, in press
31. Brünger, A.T (1992) *X-PLOR (Version 3.1)—A System for X-Ray Crystallography and NMR*, Yale University Press, New Haven, CT
32 Storici, P, Capitani, G, De Biase, D., Moser, M., John, R.A., Jansonius, J N, and Schirmer, T. (1999) Crystal structure of GABA-aminotransferase, a target for antiepileptic drug therapy. *Biochemistry* **38**, 8628–8634
33 Nakai, T, Okada, K., Akutsu, S, Miyahara, I., Kawaguchi, S., Kato, R, Kuramitsu, S., and Hirotsu, K. (1999) Structure of *Thermus thermophilus* HB8 aspartate aminotransferase and its complex with maleate. *Biochemistry* **38**, 2413–2424
34. Thompson, J.D, Higgins, D G, and Gibson, T J (1994) CLUSTAL W: improving the sensitivity of progressive multiple sequence alignment through sequence weighting, position-specific gap penalties and weight matrix choice. *Nucleic Acids Res.* **22**, 4673–4680
35. Shen, Z. and Byers, D.M. (1996) Isolation of *Vibrio harveyi* acyl carrier protein and the *fab*G, *acp*P, RT, and *fab*F genes involved in fatty acid biosynthesis. *J Bacteriol* **178**, 571–573
36 Slock, J., Stahly, D P., Han, C.-Y, Six, E W, and Crawford, I P. (1990) An apparent *Bacillus subtilis* folic acid biosynthetic operon containing *pab*, an amphibolic *trp*G gene, a third gene required for synthesis of para-aminobenzoic acid, and the dihydropteroate synthase gene. *J Bacteriol.* **172**, 7211–7226
37 Kabsch, W. and Sander, C (1983) Dictionary of protein secondary structure· pattern recognition of hydrogen-bonded and geometrical features. *Biopolymers* **22**, 2577–2637
38 Jansonius, J.N (1998) Structure, evolution and action of vitamin B6-dependent enzymes. *Curr Opin Struct Biol* **8**, 759–769
39 Yano, T., Kuramitsu, S, Tanase, S, Morino, Y, and Kagamiyama, H. (1992) Role of Asp222 in the catalytic mechanism of *Escherichia coli* aspartate aminotransferase The amino acid residue which enhances the function of the enzyme-bound coenzyme pyridoxal 5'-phosphate *Biochemistry* **31**, 5878–5887
40 Yano, T, Hinoue, Y, Chen, V.J., Metzler, D E, Miyahara, I., Hirotsu, K., and Kagamiyama, H (1993) Role of an active site residue analyzed by combination of mutagenesis and coenzyme analogue *J Mol Biol* **234**, 1218–1229
41 Inoue, K., Kuramitsu, S., Okamoto, A., Hirotsu, K., Higuchi, T., Morino, Y, and Kagamiyama, H (1991) Tyr225 in aspartate aminotransferase contribution of the hydrogen bond between Tyr225 and coenzyme to the catalytic reaction. *J. Biochem.* **109**, 570–576
42 Goldberg, J.M., Swanson, R V, Goodman, H S., and Kirsch, J F (1991) The tyrosine-225 to phenylalanine mutation of *Escherichia coli* aspartate aminotransferase results in an alkaline transition in the spectrophotometric and kinetic pK_a values and reduced values of both k_{cat} and K_m *Biochemistry* **30**, 305–312
43 Jhee, K.-H, Yoshimura, T, Kurokawa, Y., Esaki, N, and Soda, K. (1999) A stereochemical aspect of pyridoxal-5'-phosphate dependent enzyme reactions and molecular evolution. *J Microbiol Biotechnol.* **9**, 695–703
44. Jansonius, J.N and Vincent, M.G (1987) Structural basis for catalysis by aspartate aminotransferase in *Biological Macromolecules and Assemblies* (Jurnak, F A. and Mcpherson, A., eds) pp 187–285, J. Wiley and Sons, New York
45. Okamoto, A., Higuchi, T., Hirotsu, K., Kuramitsu, S, and Kagamiyama, H. (1994) X-ray crystallographic study of pyridoxal 5'-phosphate-type aspartate aminotransferases from *Escherichia coli* in open and closed form. *J Biochem.* **116**, 95–107
46. Jäger, J, Moser, M, Sauder, U, and Jansonius, J N. (1994) Crystal structure of *Escherichia coli* aspartate aminotransferase in two conformations. Comparison of an unliganded open and two liganded closed forms. *J. Mol. Biol.* **239**, 285–305
47. Miyahara, I., Hirotsu, K., Hayashi, H., and Kagamiyama, H. (1994) X-ray crystallographic study of pyridoxamine 5'-phosphate-type aspartate aminotransferase from *Escherichia coli* in three forms. *J. Biochem.* **116**, 1001–1012